Article

Simultaneous Dual-Wavelength Source Raman Spectroscopy with a Handheld Confocal Probe for Analysis of the Chemical Composition of *In Vivo* Human Skin

Yi Qi, Ruochong Zhang, Poongkulali Rajarahm, Shuyan Zhang, Amalina Binte Ebrahim Attia, Renzhe Bi,* and Malini Olivo

Cite This: *Anal. Chem.* 2023, 95, 5240−5247

Read Online

ACCESS | Metrics & More | Article Recommendations | Supporting Information

ABSTRACT: Confocal Raman spectroscopy (CRS) is a powerful tool that has been widely used for biological tissue analysis because of its noninvasive nature, high specificity, and rich biochemical information. However, current commercial CRS systems suffer from limited detection regions (450−1750 cm^{-1}), bulky sizes, nonflexibilities, slow acquisitions by consecutive excitations, and high costs if using a Fourier transform (FT) Raman spectroscopy with an InGaAs detector, which impede their adoption in clinics. In this study, we developed a portable CRS system with a simultaneous dual-wavelength source and a miniaturized handheld probe (120 mm × 60 mm × 50 mm) that can acquire spectra in both fingerprint (FP, 450−1750 cm^{-1}) and high wavenumber (HW, 2800−3800 cm^{-1}) regions simultaneously. An innovative design combining 671 and 785 nm lasers for simultaneous excitation through a compact and high-efficiency (>90%) wavelength combiner was implemented. Moreover, to decouple the fused FP and HW spectra, a first-of-its-kind precise Raman spectra separation algorithm (PRSSA) was developed based on the maximum *a posteriori* probability (MAP) estimate. The accuracy of spectra separation was greater than 99%, demonstrated in both phantom experiments and *in vivo* human skin measurements. The total data acquisition time was reduced by greater than 50% compared to other CRS systems. The results proved our proposed CRS system and PRSSA's superior capability in fast and ultrawideband spectra acquisition will significantly improve the integration of CRS in the clinical workflow.
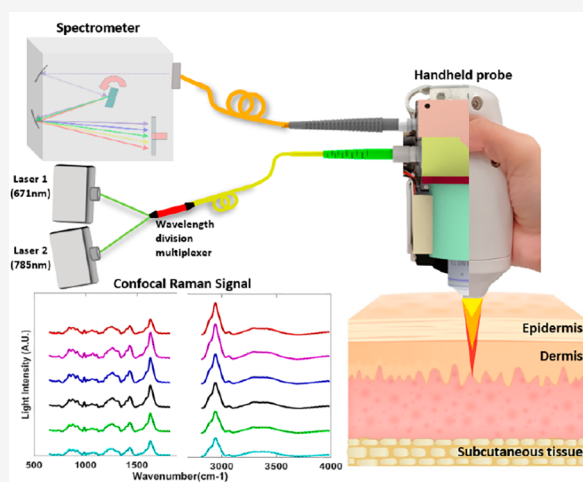
INTRODUCTION

Many optical techniques have been studied for a wide range of chemical and biomedical applications, owing to their non-invasiveness and rich light-matter interactions. For instance, fluorescence spectroscopy is based on photon absorption and subsequent emission at different energy levels by matter.[1] Optical coherence tomography utilizes backscattered photons resulting from different reflectivity patterns to obtain structural information on biological tissues.[2] Visible/infrared spectroscopy relies on optical absorption,[3] transmission, or reflection of matter.[4] Among these techniques, Raman spectroscopy, a measure of photon inelastic scattering, has exceptional specificity over other optical techniques since the resulting spectra patterns are unique for different compounds.[5] Hence, it has become a popular tool for biomedical applications such as drug design,[6] DNA/RNA analysis,[7] and disease diagnosis.[8] Confocal Raman spectroscopy (CRS) provides additional spatial resolution at the micrometer level by incorporating a confocal optical setup to suppress stray light and realize depth profiling.[9−11] Near-infrared laser is often employed as the light source for deeper penetration and less autofluorescence. The most commonly used spectrometer in Raman spectroscopy is silicon based with low noise, high sensitivity, and spectral resolution up to subnanometers.[12] Its sensitive region covers 200−1100 nm, corresponding to the fingerprint (FP) region (450−1750 cm^{-1}) of most organic chemicals, with 785 nm excitation. To get the high wavenumber (HW) region (2800−3800 cm^{-1}) for water content analysis, several Raman spectroscopy systems[13−16] adopt a dual-wavelength light source by adding a 671 nm laser[16] to extend the spectral range. However, FP and HW spectra need to be obtained separately during the acquisition by manually switching the
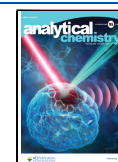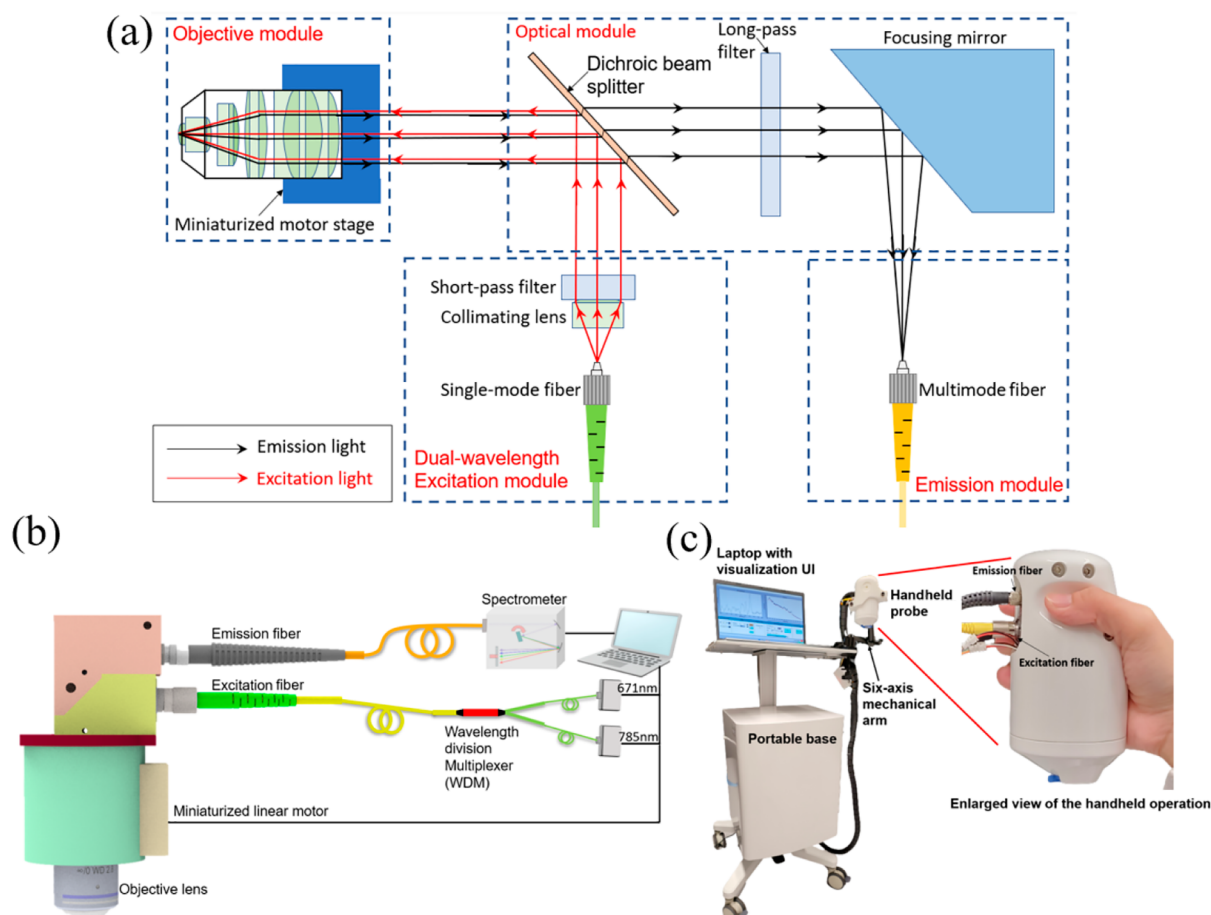
Figure 1. (a) Optical layout of handheld Raman probe, which consists of four modules: dual-wavelength light source module, optical module, objective module, and emission module. (b) Schematic of the dual-wavelength confocal Raman spectroscopy, comprising two lasers, a wavelength division multiplexer, a confocal handheld probe, a NIR spectrometer, and a laptop. (c) Photograph of the prototype of the handheld dual-band confocal Raman probe with a six-axis mechanical arm and a portable base.

laser and repeating the measurement, which may cause depth mismatch and prolonged acquisition time. This problem is even more pronounced in CRS system operation,[17] especially for *in vivo* applications. Another choice is to use a 532 nm excitation laser with a visible spectrometer that covers the 540−700 nm range.[10] Although this type of Raman spectroscopy can be used for both fingerprint and high wavenumber regions, the Raman scattering signal will be significantly influenced by the background fluorescence in the visible range. Therefore, a confocal Raman spectroscopy with a 532 nm excitation laser requires a very high power laser source (>100 mW) to increase the signal-to-noise ratio, which is not suitable for *in vivo* subject testing. Previously, we developed a CRS system with a flexible handheld probe and quasi-simultaneous dual-wavelength source solution to mitigate this problem by incorporating a fast fiber switch and dual-pass band filter.[18] However, the consecutive acquisitions by two wavelengths at each depth still required separate exposures, which is time consuming. Besides, the fiber switch had high insertion loss (loss >40%), and it increased the system complexity. Recently, Kiefer proposed a Raman fusion spectroscopy utilizing simultaneous dual-wavelength excitation and on-chip spectra fusion.[13] Univariate and multivariate data analyses were applied to analyze an aqueous dimethyl sulfoxide (DMSO) solution based on intensity variation for each pixel.[19] Although DMSO concentration was well quantified in the proof-of-

concept experiment,[20] it is not representative of skin characterization whereby the skin is made up of a complexed mixture of chromophores at different depths.

To overcome these challenges, we developed a novel and miniaturized handheld confocal Raman probe with a simultaneous dual-wavelength light source through a compact wavelength combiner. The new portable probe design, which improved the signal collection efficiency by 30%, is smaller than the first generation design by 50%,[18] which makes it one of the smallest handheld confocal Raman probes (120 mm × 60 mm × 50 mm) that can achieve depth profiling measurements on different positions of human body. More importantly, we implemented a simultaneous dual-wavelength excitation scheme by replacing the fiber switch with a more robust and efficient wavelength combiner. This is the first dual-wavelength simultaneous excitation confocal Raman spectroscopy that can cover both FP and HW regions with a single sensor and a single exposure. A first-of-its-kind precise Raman spectra separation algorithm (PRSSA) based on a maximum *a posteriori* probability (MAP) estimate was developed to decouple the on-chip fused FP and HW spectra for further unmixing and quantification. The total acquisition time can be shortened by greater than 50%, compared to commercial and previously reported CRS systems,[18] which require two consecutive excitations and repeated measurements. The performance of our new probe and PRSSA was then validated

by both a phantom experiment and *in vivo* human skin measurement.

SYSTEM DESIGN AND IMPLEMENTATION

Instrument Setup. In our first generation probe design, we reported a handheld Raman probe with a fiber switch, which still required two consecutive exposures to obtain the FP and HW spectra in sequence, thus could only achieve quasi-simultaneous measurement.[18] Although it has good performance, there is a big technical gap from a real-simultaneous dual-wavelength excitation system, which would take only a single exposure to obtain both FP and HW spectra. Meanwhile, the fiber switch is not robust enough with a high insertion loss (>40%). Therefore, a brand new optical design of the handheld probe was developed, as shown in Figure 1(a). The light source module is a fiber-coupled input of light, which consists of two wavelengths (671 and 785 nm) laser beams. A collimating lens is used to collimate the laser beam from the single-mode fiber, and a dual-passband laser cleaning filter (DPLCF) eliminates the fluorescence or other unwanted wavelengths from the fiber. The dichroic beam splitter is placed after the DPLCF to reflect the dual-wavelength light beam to the objective lens. While the dual-laser beam shoots on the object, both the Rayleigh scattering and the Raman scattering will be collected by the objective module. A majority (~90%) of Rayleigh scattering will be reflected by the dichroic beam splitter to the light source module, while the remaining 10% will be blocked by the long-pass filter with a cut-on wavelength of 809 nm. Instead of using a lens, a focusing mirror after the long-pass filter will reflect and focus the emitted Raman signals into a multimode fiber. With this new design, both the excitation fiber and signal collection fiber can be placed at the same side, instead of being positioned perpendicular to each other in the previous design, which reduces the size by 50% and makes the probe more convenient for handheld operation. Furthermore, different from other handheld Raman spectroscopy systems which normally require a high power laser source (>50 mW), owing to the high signal collection efficiency of the probe, our system can use low power lasers (5−20 mW), which is safe for *in vivo* biological tissues.[21]

Figure 1(b) shows the schematic of the simultaneous dual-wavelength source CRS system. Compared with the generation 1 design, the fiber array multiplexing module was replaced by a high transmission efficiency (>90%), 2-to-1 wavelength combiner multiplexer (WDM) (NR75A1, Thorlabs), and the two CW lasers of 671 and 785 nm were shot simultaneously through the single-mode fiber (SMF) with a 0.12 numerical aperture (NA) and combined by the WDM into the single-mode fiber. A microscope objective lens (NIR Apo 60× 1.0 W, Nikon) is mounted on a customized miniaturized linear motor to implement depth profiling. The movement of the motor can be controlled by the laptop, and the position of the objective lens will be autocalibrated before each measurement to ensure the accuracy of the confocal depth. The delivered power of 671 and 785 nm lasers are 7 and 19 mW, respectively. The emission fiber connects to a near-infrared spectrograph (Kymera 193i) with a back-illuminated CCD camera (iDus 416, Andor Technology). The response signals for different wavelength lasers will be calibrated with the quantum efficiency curves that are provided by Andor Technology. The spectra data are acquired by the laptop for further processing.

Photographs of the handheld probe and the prototype of the system for clinical studies are shown in Figure 1(c). The handheld probe is mounted on a six-axis mechanical arm, which is attached to a portable base, where the rest of the system components are housed. The arm and base enable the probe to be placed at any position and angle, allowing depth profile data to be acquired from any part of the body. This minimizes movement during measurement as well.

Experimental Section. A water immersion objective with high magnification and NA is used to increase the throughput of the CRS system. Conventionally an oil or water immersion objective is placed upright in a benchtop system,[11] as it requires a stable base for the liquid to sit in, which is not always practical in a clinical setting, so it is very common for the probe to be in a tilted position to image various parts of the skin in the body. To overcome this, we developed a skin adhesive with a small reservoir in the center to hold the water as shown in Figure 1(c). The diameter of the circular reservoir matched that of the objective opening on the probe casing. In this way, the probe casing can be attached to the skin adhesive to prevent the spillage of water. The skin adhesive is made of disposable plastic, which is cost effective and safe. After placing the skin adhesive on the region of interest (ROI), i.e., cheek, the three joints of the mechanical arm are unlocked, and the protruding end of the probe is placed on the adhesive. Once this is done, the three joints of the mechanical arm can be locked. Water is then filled from the opening in the probe with a syringe and needle. With this novel setup and workflow, the handheld confocal Raman probe can measure any part of a body in a stable and robust way, leading to good data quality. The detailed workflow with the experimental illustration is described in Supporting Information, Section I.

Data Preprocessing. While the excitation light illuminates biological tissues, the Raman scatter will be affected by broad background noises. The background interferences, including the intrinsic fluorescence, and other stray lights, are usually several orders of magnitude stronger than Raman signals. Hence, the elimination of the background noise from the raw signal before data processing is necessary. Fortunately, there is a significant shape difference between the broadband fluorescence background and the sharp Raman peaks. According to the background noise subtraction methods published in literature,[22−24] we use polynomial fitting (PF) as the baseline estimation algorithm. Since dual-wavelength lasers (671 and 785 nm) were used in this study for the excitation of Raman scattering, the Raman spectra of the two lasers will be superimposed within the 810 to 950 nm wavelength region, with the PF order being 9 for the baseline estimation. Therefore, the corresponding wavenumber of the Raman spectra after the background removal will be allocated at the FP region (450−1750 cm^{-1}) and HW region (2800−3800 cm^{-1}) separately.

Here, we have developed a new algorithm, PRSSA, for accurate separation of the superimposed FP-HW Raman spectra. To validate the algorithm, we also acquired FP and HW Raman spectra with consecutive 671 and 785 nm excitations as the ground truth of the separated spectra for comparison. While the raw data have been acquired by Raman spectroscopy, we used the MATLAB polynomial curve fitting function to determine the best PF order of FP, HW, and FP-HW Raman spectra curves separately. The Raman spectra were calculated by subtracting the PF baseline from raw data.

We proposed the PRSSA, which can achieve simultaneous dual-band Raman spectra acquisition and separation with our dual-wavelength source handheld CRS. While the detailed mathematical model and derivation process of the algorithm is described in Supporting Information, Section II, the concluding equation with the workflow of the application of the PRSSA in a dual-wavelength source Raman spectrometer is described here.

The PRSSA is developed based on the MAP estimate. MAP is a point estimate of a difficult-to-observe quantity obtained from empirical data.[25,26] MAP incorporates the prior distribution of the quantities to be estimated in it, or in other words, it uses some preknowledge data to predict unknown data under defined conditions. Based on the MAP algorithm, the PRSSA requires three premeasurement reference signals to decouple the dual-wavelength excitation signal into two single-wavelength excitation results. The HW and FP Raman spectra excited by 671 and 785 nm are fused in the same wavelength region (810−950 nm), when measured by the same Si-based spectrometer. This feature provides the opportunity to differentiate the individual Raman spectra of HW region excited by 671 nm and the FP region excited by 785 nm from a fused spectrum. The workflow diagram of the spectra separation is shown in Figure 2. Before using the
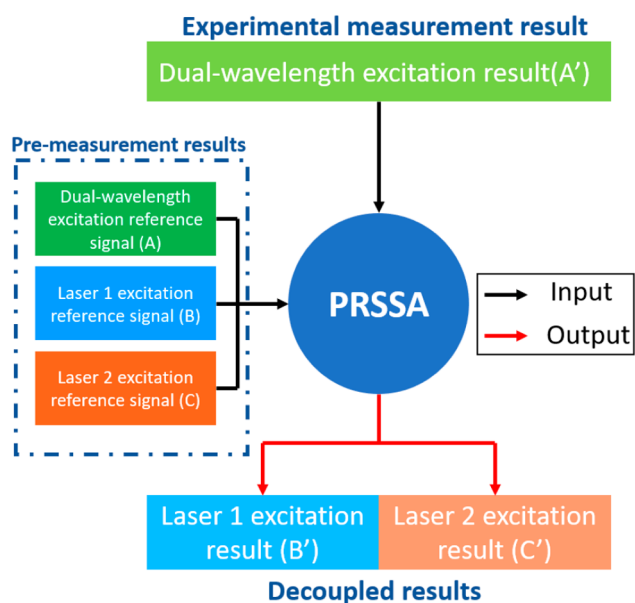

Figure 2. Workflow of the application of precise Raman spectra separation algorithm (PRSSA).

PRSSA, it is necessary to confirm the object has the following features:

(a) The object must consist of fixed components, which means the concentration of each component can be changed, but the variety of these components must be the same in different samples. In this case, the wavenumbers of feature peaks in the Raman spectra will not be changed. Therefore, a dual-wavelength excitation Raman spectra can be decoupled into two spectra while each one contains the feature peaks of a single-wavelength excitation Raman spectra.

(b) The premeasurement results have no limitations on the concentrations of the constituents of the target.

However, three reference signals A, B, and C must be acquired from the same sample, which means the reference signal must meet the following:

$$A = B + C$$

(c) While the composition of the object has been changed, the reference signals must be reacquired.

Once the above features can be met, the decoupling of the dual-wavelength excitation result (A') can proceed with PRSSA with the following steps:

(i) Place the probe on the surface of a reference object and turn on both lasers to measure the dual-wavelength excitation reference signal (A).

(ii) Turn off laser 2 and measure the excitation reference signal of laser 1 (B).

(iii) Turn off laser 1 and turn on laser 2, then measure the excitation reference signal of laser 2 (C).

(iv) Remove the reference object and place the probe on the surface of the ROI, then turn on both lasers to acquire dual-wavelength excitation (A').

(v) Use the polynomial fitting method to eliminate the background noise of A, B, C, and A' and then use them to calculate the laser 1 excitation result (B') and laser 2 excitation result (C') by PRSSA.

Here, we provide the conclusion, while $b_n > 5c_n$:

$$b_n' = b_n + \left(\frac{b_n}{a_n} + \frac{b_n c_n}{a_n^2}\right)(a_n' - a_n)$$

$$c_n' = c_n + \left(\frac{c_n}{a_n} - \frac{b_n c_n}{a_n^2}\right)(a_n' - a_n) \tag{1}$$

While $c_n > 5b_n$:

$$b_n' = b_n + \left(\frac{b_n}{a_n} - \frac{b_n c_n}{a_n^2}\right)(a_n' - a_n)$$

$$c_n' = c_n + \left(\frac{c_n}{a_n} + \frac{b_n c_n}{a_n^2}\right)(a_n' - a_n) \tag{2}$$

In other situations:

$$b_n' = b_n + \left(\frac{b_n}{a_n}\right)(a_n' - a_n)$$

$$c_n' = c_n + \left(\frac{c_n}{a_n}\right)(a_n' - a_n) \tag{3}$$

where a_n, b_n, c_n, and a_n' are the values of A, B, C, and A', respectively, at wavelength n, while b_n' and c_n' are the values of the extraction result of B' and C', respectively, at wavelength n.

■ RESULTS AND DISCUSSION

Phantom Experiment with Acetic Acid and Ethanol Mixture. We first validated the performance of PRSSA using a mixture solution of acetic acid (AA) and ethanol. From eqs 1−3, we must first acquire a group of reference signals: A, the Raman signal of the mixture solution with both excitation lasers, B, the Raman signal of the mixture solution with the first excitation laser, and C, the Raman signal of the mixture solution with the second excitation laser. Therefore, we
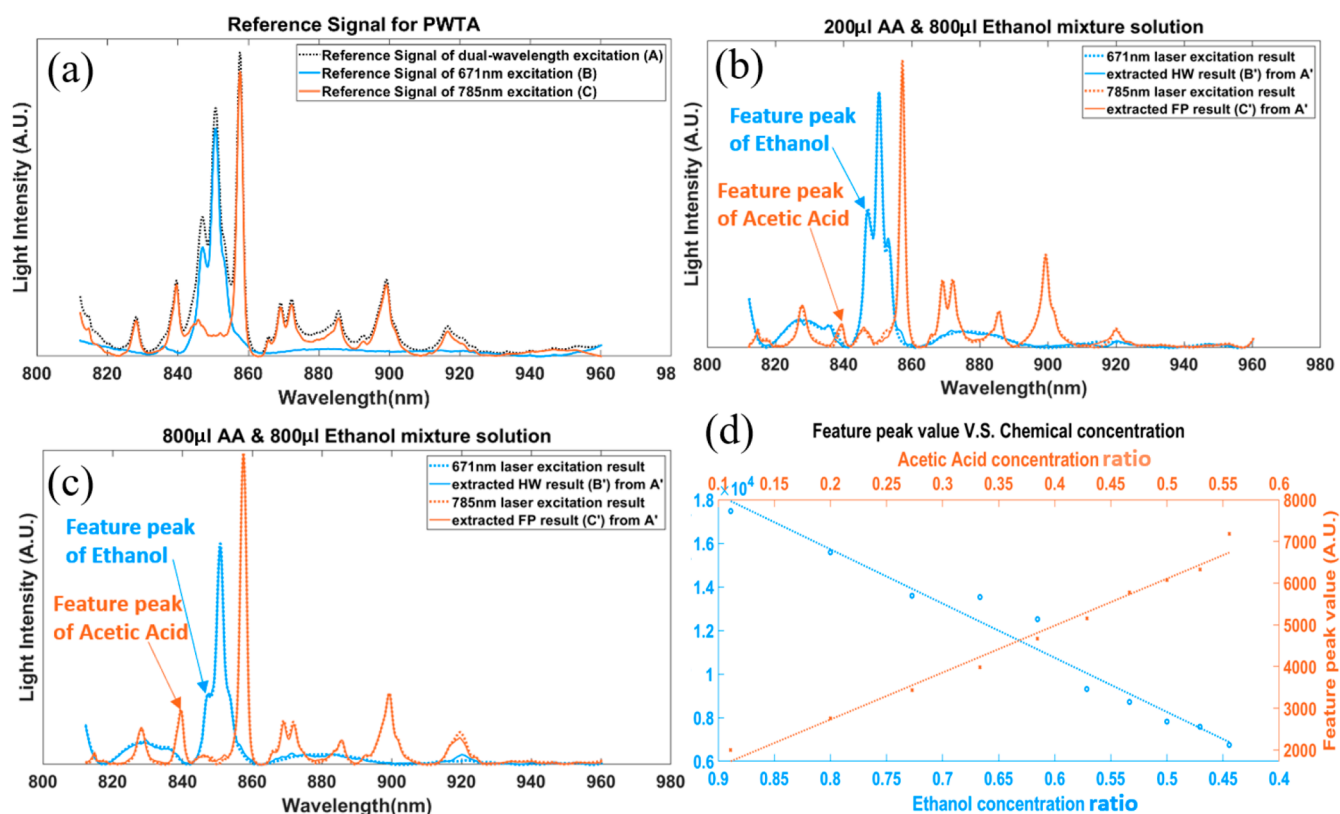
Figure 3. Fluorescence background free results of acetic acid and ethanol in different concentrations. (a) Reference signals for PRSSA, which were tested on pure acetic acid (AA) and ethanol with 671 nm laser, 785 nm laser, and dual-wavelength laser. (b) Extracted results of a 200 μL AA and 800 μL ethanol mixture solution from dual-wavelength excitation with PRSSA, compared with the tested results from single-wavelength excitation. (c) Extracted results of a 800 μL AA and 800 μL ethanol mixture solution from dual-wavelength excitation with PRSSA, compared with that from single-wavelength excitation. (d) Feature peak value of the FP (orange ×) and HW (blue ○) extracted results with different concentration of AA and ethanol in a mixture solution, and the fitting line of these results.

Table 1. Correlation Ratios between Single-Wavelength Excitation Result and Extracted FP and HW Results of Mixture Solution in Mixtures of Different Concentrations of Acetic Acid (AA) and Ethanol (E)

Correlation ratio	100 μL AA and 800 μL E	200 μL AA and 800 μL E	300 μL AA and 800 μL E	400 μL AA and 800 μL E	500 μL AA and 800 μL E
671 nm/HW	99.53%	99.80%	99.61%	99.78%	99.69%
785 nm/FP	99.40%	99.66%	99.59%	99.53%	99.61%
Correlation ratio	600 μLAA and 800μL E	700 μL AA and 800 μL E	800 μL AA and 800 μL E	900 μL AA and 800 μL E	1000 μL AA and 800 μL E
671 nm/HW	99.67%	99.68%	99.65%	99.46%	99.64%
785 nm/FP	99.75%	99.80%	99.72%	99.71%	99.71%

acquired a Raman signal of 1:1 AA and the ethanol mixture solution with 671 nm, 785 nm, and dual-wavelength excitation lasers to get a group of reference signals: A is the Raman signal that is excited by dual-wavelength excitation, B the Raman signal that is excited by a 671 nm laser, and C the Raman signal that is excited by a 785 nm laser. It should be noted that once the reference signals A, B, and C have been acquired, they can be used for the same mixture with different concentrations of each component without affecting the validity of the algorithm. Furthermore, for reference signal acquisitions, there is no special requirement of the concentration of each component. However, if the composition of the mixture solution changes, the reference signals must be reacquired on the new mixture solution.

After the reference signals were obtained, the mixture solution with ten different concentration combinations (800 μL ethanol and 100−1000 μL AA with 100 μL step size) were

tested with dual-wavelength excitation to determine the combination signal A'. The PRSSA was then used for the extraction of the FP (C') and HW (B') Raman signals from the combined signal. As shown in Figure 3(b) and (c), when the volume of AA increased from 200 to 800 μL, the feature peak of AA increased at 785 nm excitation (855−860 nm region) and the feature peak of ethanol decreased at 671 nm excitation (845−855 nm region). Meanwhile, the ground truth spectra are plotted as dotted lines, and the correlation ratios between the extracted spectra and the ground truth were calculated. Table 1 summarizes the correlation ratios obtained from the ten concentration combinations of the AA−ethanol mixture. More details and figures can be found in Supporting Information, Section III. The results illustrate that PRSSA has greater than 99% accuracy for the FP and HW spectra separation from a fused spectra (Table 1). Figure 3(d) shows the feature peak values in the extracted FP and HW spectra for

the 10 mixture solutions with different ethanol and AA concentrations. It can be seen that the value of the AA feature peak at 785 nm excitation increased with the concentration of AA while the ethanol feature peak at 671 nm excitation decreased. When using first order polynomial fitting to fit these results in a linear model, which are shown as dotted lines in Figure 3(d), the R^2 values of the fitted lines are 0.9606 for ethanol and 0.9821 for AA, demonstrating the linear correlation between the concentration and the Raman peak value.

***In Vivo* Skin Measurement.** As human skin is made up of a variety of complex compounds, the reference signal for every pure component is tedious to obtain. Therefore, we directly used 671 nm, 7 mW excitation (B), 785 nm 19 mW excitation (C), and dual-wavelength excitation (A) Raman signals of healthy human skin as the reference signals. (The recruitment and measurement of healthy volunteers were approved by the A*STAR Institutional Review Board (IRB), with reference number 2021-098. The protocol title is "Testing and validation of noninvasive optical technologies for translational biophotonics innovation platform".) This illustrates the convenience of PRSSA in which the reference signal is not restricted by special requirements. In Figure 4(a), the fluorescence-subtracted dual-wavelength excitation Raman signal (A') of human skin is shown, which is the raw data acquired by our prototype with a 1 s exposure time. After PRSSA separation, two groups of spectra could be recovered from the raw data, as shown in blue and orange, representing the Raman signal generated by 671 nm excitation (B') and 785 nm excitation (C'), respectively. The ground truth single wavelength excitation results were also measured individually for comparison, as shown in the black dotted curve in Figure 4(a). The correlations between PRSSA recovered HW/FP spectra (blue/orange solid curves) and the ground truth single wavelength excitation spectra (black dotted curve) are 99.77% and 99.44%, respectively.

Figure 4(b) further shows the FP and HW fluorescence-subtracted Raman spectra of human skin at different depths, which is enabled by the confocal depth profiling capability of the prototype. Chemistry component information of the skin in different depths can be determined by the signal intensities in different bands, such as the Amide I band within 1600−1700 cm^{-1}. Proteins and lipids are related to CH_2 bending, which can be found within 1400−1500 cm^{-1}, and 1200−1350 cm^{-1} is Amide III band (v(C−C) vibrational band failing is within 800−1050 cm^{-1}). Similarly, in the HW region, the O−H band from water (3350−3550 cm^{-1}) and the CH_3 band due to keratin (2910−2965 cm^{-1}) were clearly shown in the spectra, which can be used to determine the thickness of the stratum corneum of the skin.[27] According to the literature, the water content in the skin also can be calculated by the water−protein ratio, which is the peak value in the O−H band region (3350−3550 cm^{-1}) divided by the peak value in the keratin region (2910−2965 cm^{-1}). These Raman scattering peaks and features could be detected, demonstrating the high performance of the PRSSA in the FP region. The black dotted curves are the ground truth spectra acquired by single-wavelength excitation. It has been clearly shown that the decoupled dual-wavelength source confocal Raman spectra have high correlation with the corresponding ground truth.
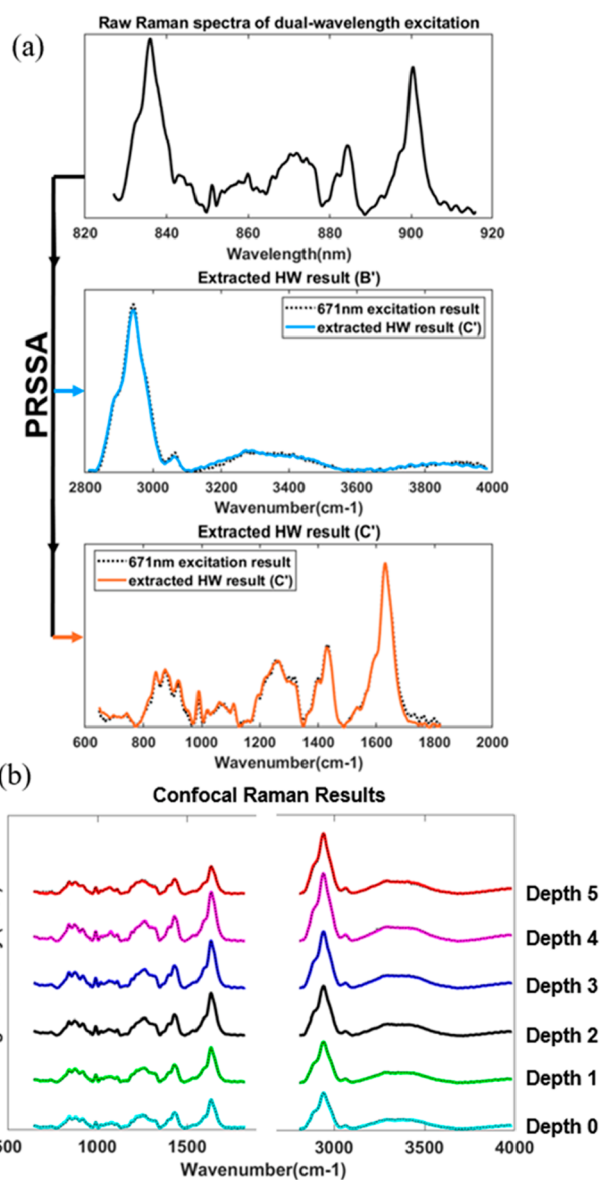

Figure 4. (a) Extracted spectra from the raw signal by PRSSA, representing the Raman spectra with the 671 nm excitation laser (blue) and 785 nm excitation laser (orange). (b) Extracted FP and HW Raman spectra at different depths, Depth 0 is the skin surface, and the reference spectra are shown as black dotted curves.

■ CONCLUSION

In conclusion, a simultaneous dual-wavelength source fiber-based confocal Raman spectroscopy (CRS) system together with a precise Raman spectra separation algorithm (PRSSA) have been presented. The acquisition of in-chip fused FP and HW Raman spectra of *in vivo* human skin and the precise spectra separation by PRSSA have been demonstrated for the first time. In the proposed system, 671 and 785 nm laser sources are coupled into a handheld confocal probe by a high efficiency wavelength division multiplexer to achieve simultaneous excitation through a single-mode fiber. The overlapped Raman signals from both lasers are recorded by a silicon-based dispersive spectrometer; then, they are separated into FP and HW regions by PRSSA. The recovered FP and HW spectra have high fidelity (correlation >99%) compared with the

corresponding ground truth. Compared with other dual-wavelength source Raman systems, our method realized true simultaneous dual-band spectra acquisition and separation, which reduced system and operation complexities significantly. Meanwhile, the acquisition time can be shortened by greater than 50%, compared to the conventional wavelength-switching excitation Raman system. Furthermore, the dimension of the new generation handheld probe has been reduced by greater than 50% with 30% improvement of signal collection efficiency compared with our first generation design,[18] which makes the system more compact and versatile for different measurement sites in different application scenarios, such as skin sites including the face, abdomen, forearm, and leg. The system has big potential to be used for the diagnosis of various skin diseases, for example, eczema or skin cancer, as long as corresponding spectral databases have been developed.

PRSSA has been developed for the first time based on the MAP estimate algorithm. This new algorithm can be used to decouple overlapped signals with only one group of reference signals. As long as the chemical composition of the object is not changed, the reference signal can be reused to determine the concentration of each component of the object. The accuracy of the algorithm has been validated by comparing the decoupled spectra with the corresponding ground truth spectra from a mixture solution of AA and ethanol. This algorithm has great potential to become a reference-free algorithm with database development and artificial intelligence.

With the handheld probe, we have also successfully acquired and separated the FP and HW confocal Raman spectra of *in vivo* human skin with a single exposure at each depth. The accuracy is greater than 99% along all depths. The simultaneous dual-wavelength measurement can eliminate the depth mismatch and mitigate patient's discomfort caused by prolonged acquisition time. The total scanning time is about 1 min for 10 depths, which saves greater than 50% of the time compared with the commercial dual-band Raman spectroscopy system.

Collectively, with robust optical implementation and high ease of use, the system has great potential to become a valuable point-of-care technology in routine clinical workflows, especially in dermatological applications. Moreover, the PRSSA provides a new solution to decouple two overlapped spectra, which can be easily adopted by other confocal Raman spectroscopy systems as well, to facilitate commercialization of an ultrawideband high sensitivity Raman system for biomedical and pharmaceutical applications.

■ ASSOCIATED CONTENT

Ⓢ Supporting Information

The Supporting Information is available free of charge at https://pubs.acs.org/doi/10.1021/acs.analchem.2c05065.

> Sections I, II, and III: Experimental workflow, derivation process of PRSSA, and phantom experiment with acetic acid and ethanol mixture (PDF)

■ AUTHOR INFORMATION

Corresponding Author

Renzhe Bi − *Institute of Bioengineering and Bioimaging, A*STAR, Singapore 138667, Singapore;* ⓞ orcid.org/0000-0001-7173-064X; Email: bi_renzhe@ibb.a-star.edu.sg

Authors

Yi Qi − *Institute of Bioengineering and Bioimaging, A*STAR, Singapore 138667, Singapore*

Ruochong Zhang − *Institute of Bioengineering and Bioimaging, A*STAR, Singapore 138667, Singapore;* ⓞ orcid.org/0000-0002-5611-6155

Poongkulali Rajarahm − *Institute of Bioengineering and Bioimaging, A*STAR, Singapore 138667, Singapore*

Shuyan Zhang − *Institute of Bioengineering and Bioimaging, A*STAR, Singapore 138667, Singapore;* ⓞ orcid.org/0000-0002-1286-4856

Amalina Binte Ebrahim Attia − *Institute of Bioengineering and Bioimaging, A*STAR, Singapore 138667, Singapore*

Malini Olivo − *Institute of Bioengineering and Bioimaging, A*STAR, Singapore 138667, Singapore*

Complete contact information is available at:
https://pubs.acs.org/10.1021/acs.analchem.2c05065

Author Contributions

Renzhe Bi designed the research. Yi Qi and Ruochong Zhang performed data analysis and algorithm development. Poonkulali Rajarahm performed experiments. Yi Qi, Ruochong Zhang, Shuyan Zhang, and Amalina Binte Ebrahim Attia wrote the manuscript. Malini Olivo provided critical instructions.

Notes

The authors declare no competing financial interest.

■ ACKNOWLEDGMENTS

■ REFERENCES

(1) Lakowicz, J. R. Introduction to Fluorescence. In *Principles of Fluorescence Spectroscopy*; Springer, 1999; pp 1−23.

(2) Fujimoto, J.; Drexler, W. Introduction to Optical Coherence Tomography. In *Optical Coherence Tomography*; Springer, 2008; pp 1−45.

(3) Jentoft, F. C. *Advances in catalysis* **2009**, *52*, 129−211.

(4) Wahr, J. A.; Tremper, K. K.; Samra, S.; Delpy, D. T. *Journal of cardiothoracic and vascular anesthesia* **1996**, *10* (3), 406−418.

(5) Shen, H.; Rösch, P.; Pletz, M. W.; Popp, J. *Anal. Chem.* **2022**, *94* (13), 5375−5381.

(6) Paudel, A.; Raijada, D.; Rantanen, J. *Advanced drug delivery reviews* **2015**, *89*, 3−20.

(7) Sato, H.; Maeda, Y.; Ishigaki, M.; Andriana, B. *Biomedical Applications of Raman Spectroscopy.* **2000**, 1−12.

(8) Schmitt, M.; Popp, J. *J. Raman Spectrosc.* **2006**, *37* (1−3), 20−28.

(9) Caspers, P. J.; Bruining, H. A.; Puppels, G. J.; Lucassen, G. W.; Carter, E. A. *Journal of investigative dermatology* **2001**, *116* (3), 434−442.

(10) Liu, Y.; Lunter, D. J. *Int. J. Pharm.* **2022**, *616*, 121561.

(11) Caspers, P. J.; Lucassen, G. W.; Puppels, G. J. *Biophys. J.* **2003**, *85* (1), 572−580.

(12) Cooper, J. B.; Marshall, S.; Jones, R.; Abdelkader, M.; Wise, K. L. *Appl. Opt.* **2014**, *53* (15), 3333−3340.

(13) Kiefer, J. *Anal. Chem.* **2019**, *91* (3), 1764−1767.

(14) Kiefer, J. *Analytical chemistry* **2019**, *91* (3), 1764−1767.

(15) Ye, J.; Tian, Z.; Hu, Y.; Wei, H.; Li, Y.; Zhao, Y.; Zou, M. *Appl. Opt.* **2021**, *60* (12), 3540−3548.

(16) Masson, L. E.; O'Brien, C. M.; Pence, I. J.; Herington, J. L.; Reese, J.; Van Leeuwen, T. G.; Mahadevan-Jansen, A. *Analyst* **2018**, *143* (24), 6049−6060.

(17) Gallardo, A.; Spells, S.; Navarro, R.; Reinecke, H. *J. Raman Spectrosc.* **2007**, *38* (7), 880−884.

(18) Zhang, R.; Bi, R.; Ho Jun Hui, C.; Rajarahm, P.; Dinish, U. S.; Olivo, M. *ACS Sens* **2021**, *6* (8), 2960−2966.

(19) Chen, X.; Allen, H. C. *J. Phys. Chem. B* **2010**, *114* (46), 14983−14988.

(20) Okutan, L.; Kongstad, K. T.; Jäger, A. K.; Staerk, D. *J. Agric. Food Chem.* **2014**, *62* (47), 11465−11471.

(21) Motz, J.; Gandhi, S.; Scepanovic, O.; Haka, A.; Kramer, J.; Dasari, R.; Feld, M. *J. Biomed Opt* **2005**, *10* (3), 031113.

(22) Cadusch, P. J.; Hlaing, M. M.; Wade, S. A.; McArthur, S. L.; Stoddart, P. R. *J. Raman Spectrosc.* **2013**, *44* (11), 1587−1595.

(23) Chen, S.; Kong, L.; Xu, W.; Cui, X.; Liu, Q. *IEEE Access* **2018**, *6*, 67709−67717.

(24) Kiselev, R.; Schie, I. W.; Askrabic, S.; Krafft, C.; Popp, J. *Biomedical Spectroscopy and Imaging* **2016**, *5* (2), 115−127.

(25) Greig, D. M.; Porteous, B. T.; Seheult, A. H. *Journal of the Royal Statistical Society: Series B (Methodological)* **1989**, *51* (2), 271−279.

(26) Levitan, E.; Herman, G. T. *IEEE Transactions on Medical Imaging* **1987**, *6* (3), 185−192.

(27) Egawa, M.; Hirao, T.; Takahashi, M. *Acta dermato-venereologica* **2007**, *87* (1), 4−8.